



ELSEVIER

Contents lists available at ScienceDirect

International Journal of Adhesion & Adhesives

journal homepage: www.elsevier.com/locate/ijadhadh

Adhesion performance of PSA–clay nano-composites by the *in-situ* polymerization and mechanical blending

Jin-Kyoung Oh, Cho-Hee Park, Seung-Woo Lee, Ji-Won Park, Hyun-Joong Kim*

Laboratory of Adhesion and Bio-Composites, Program in Environmental Materials Science, Seoul National University, Daehak-Dong, Gwanak-Gu, Seoul 151-921, Republic of Korea

ARTICLE INFO

Article history:

Accepted 11 June 2013

Available online 25 September 2013

Keywords:

Adhesion performance

Nanoclay

in-situ

Mechanical blend

Emulsion polymerization

Acrylic adhesive

ABSTRACT

The synthesis and characterization of acrylic polymer/Na-montmorillonite (Na-MMT) clay nano-composites pressure sensitive adhesives (PSA) are researched. The PSA/clay nano-composites were synthesized by *in-situ* emulsion polymerization and mechanical blending. And then, different amounts of nanoclay were dispersed in 2-ethylhexyl acrylate (2-EHA)/*n*-butyl acrylate (BA)/methyl methacrylate (MMA)/acrylic acid (AA) monomer mixture, which was synthesized using *in-situ* emulsion polymerization technique. Morphological observation was carried out using X-ray diffraction (XRD) and field emission scanning electron microscope (FE-SEM). Viscoelastic properties of PSA/clay nano-composites were analyzed using advanced rheometric expansion system (ARES). The adhesion performances of synthesized PSA/clay nano-composites were determined by measurements of peel strength, probe tack and shear adhesion failure temperature.

© 2013 Published by Elsevier Ltd.

1. Introduction

Acrylic pressure-sensitive adhesives (PSAs) have been developed rapidly because of their versatility, ease of application, optically clarity, oxidative and ultraviolet (UV) resistance, migration resistance, low toxicity and low cost raw materials [1]. Acrylic PSAs, in general, are copolymerized with low T_g monomers such as *n*-butyl acrylate and 2-ethylhexyl acrylate for tackiness and high T_g monomers for cohesive strength. To increase the mechanical properties and thermal stability, cross-linkable monomers have been used because the general acrylic PSAs have linear structures. Monomer composition greatly influences on the adhesion performances of acrylic PSAs [2].

Emulsion polymerizations are widely used in a variety of applications because of not only limitations of heat transfer in the large scale reactors [3] and strict environmental regulations such as EPA Clean Air Act, but also high cost of solvent-borne acrylic PSAs and slow coating line speed. For this reason, solvent-borne acrylic PSAs have been replaced with water-borne acrylic PSAs (emulsion PSAs). Despite of the aggressive effort to replace them, solvent-borne acrylic PSAs are still used in the field of high-performance tapes and label. Because water-borne acrylic PSAs reveal lower adhesion performance, shear strength and heat resistance than that of solvent-borne acrylic PSAs.

To exploit the new class of high performance PSAs based on acrylic emulsion PSAs, various fillers have been added to PSAs to give enhanced properties [4–6]. Among them, addition of a small amount of nanoclay into a polymer matrix exhibit increased modulus, decreased thermal expansion coefficients, reduced gas permeability and increased solvent resistance when compared to the polymers alone [7–9]. The enhanced properties of polymer–clay nano-composites would also be desirable in the PSAs field. However, these improved properties of composites depend on the dispersed status of nanoclay in the polymer matrix [10]. In general, two idealized polymer–clay structures are possible: intercalated and exfoliated [7,11]. In intercalated nano-composites, the polymer molecules enter to the interlayer of nanoclay. The nanoclay layers maintain their order and the increasing spacing between layers can be seen by X-ray diffraction (XRD). In exfoliated nano-composites, the individual layers of nanoclay were dispersed into the polymer matrix. The individual layers in polymer matrix resulting from extensive polymer penetration and delamination of the silicate crystallites. The greatest improved properties are observed in exfoliated nano-composites [12–14].

Polymer–clay nano-composites can be manufactured using various processes; solution intercalation, melt intercalation [15], *in-situ* polymerization and template synthesis [16]. Ray and Okamoto published the synthesis of PLA-layered silicate nano-composites. They found that addition of layered silicate nanoclay to PLA matrix improves mechanical properties, heat distortion temperature, gas permeability compared to pure PSA [17]. Meneghetti and Qutubuddin also published a paper dealing with polymethylmethacrylate–montmorillonite

* Corresponding author. Tel.: +82 2 880 4794; fax: +82 2 873 2318.
E-mail address: hjokim@snu.ac.kr (H.-J. Kim).

(PMMA–MMT) nano-composites by emulsion polymerization. They showed that the particle morphology and properties were affected by the nature of intercalation between the clay surfaces [18]. Wang et al. studied waterborne nano-composite PSA reinforced with carbon nanotubes to improve electrical conductivity and to increase the energy of adhesion with maintains optical transparency [5]. There are several studies that the emulsion polymerization has been based on high glass transition temperature (T_g) polymers such as PMMA, PS and PAN [6,19–21]. They are not associated to PSAs applications.

In this paper, we prepare the PSA–clay nano-composites by *in-situ* emulsion polymerization and mechanical blend. First, a series of 2-ethylhexyl acrylate (2-EHA)/*n*-butyl acrylate (BA) copolymers functionalized with methylmethacrylate (MMA) and acrylic acid (AA) were synthesized by semicontinuous emulsion polymerization. The influence of the 2-EHA/BA ratio on the adhesion performances of acrylic emulsion PSAs was studied. Next, polymer–clay nano-composites were prepared by *in-situ* emulsion polymerization and by the blending with Na–MMT clay. The morphological properties, viscoelastic properties and adhesion performances were compared to PSA–clay nano-composites produced by two different procedures.

2. Experimental

2.1. Materials

2-Ethylhexyl acrylate (2-EHA, Samchun Pure Chemical, Republic of Korea), *n*-butyl acrylate (BA, Samchun Pure Chemical, Republic of Korea), methyl methacrylate (MMA, Samchun Pure Chemical, Republic of Korea) and acrylic acid (AA, Samchun Pure Chemical, Republic of Korea) were used without any purification. The initiator, ammonium persulfate (APS), was obtained from Hebei Jiheng Group Co., Ltd., PR China. Sodium dodecyl sulfate (SDS, Junsei Chemical Co., Ltd, Japan) was used as surfactant. Its activity in water is 34.5–38.5% by weight. The buffer, sodium pyrophosphate decahydrate (Samchun Pure Chemical, Republic of Korea), was used to control pH of acrylic emulsion PSAs. Aqueous ammonia (NH₄OH, 28%, Sungjin, Republic of Korea) was used neutralization. Nanoclay (Closite[®] Na⁺) was purchased from Southern Clay Products, Inc. (Gonzales, TX, USA). Nanoclay is montmorillonite modified with quaternary ammonium salt. This is an additive to improve various physical properties, such as mechanical property reinforcement, heat, shear resistance, and so on. Table 1 shows basic properties of nanoclay used in this study.

2.2. Preparation of acrylic pre-emulsion PSA

Deionized (DI) water, surfactant, initiator and buffer were homogeneously mixed at about 60 °C in the four neck flask under reflux. Apart from this mixture, 2-EHA, BA, MMA and AA were charged into DI water solved with surfactant, chain transfer, isopropyl alcohol (IPA), and then pre-emulsion was prepared for 90 min at room temperature until the pre-emulsion became milky white color. The various monomer compositions used to synthesize the acrylic emulsion PSAs are shown in Table 2. The 2-EHA/BA ratio in the monomer compositions were 15/75, 30/60, 45/45,

Table 1
The basic properties of Closite[®] Na⁺.

	Closite [®] Na ⁺
Modifier concentration (meq/100 g clay)	92.6
Moisture content (%)	4–9
Density (g/cm ³)	2.86
XRD d ₀₀₁ (Å)	11.7

Table 2
Acrylic pre-emulsion PSAs composition.

Sample ^b	Monomer charged per total monomer ^a			
	2-EHA	BA	MMA	AA
2-EHA 15	15	75		
2-EHA 30	30	60		
2-EHA 45	45	45	8	2
2-EHA 60	60	30		
2-EHA 75	75	15		

^a Monomer charged based on the total weight of the total monomers.

^b Total weight of monomer mixture was 220 g.

60/30 and 75/15 wt% based on the total monomer. The MMA and AA content were constantly fixed at 8 and 2 wt%, respectively. Each PSA was named 2-EHA 15, 2-EHA 30, 2-EHA 45, 2-EHA 60 and 2-EHA 75 as the content of the 2-EHA proportion.

2.3. Synthesis of acrylic emulsion PSAs reinforced with nanoclay

Among the various compositions, 2-EHA 45 was selected to synthesize acrylic emulsion PSAs reinforced with nanoclay using two procedures, *in-situ* polymerization and mechanical blending.

2.3.1. *In-situ* semibatch emulsion polymerization

The synthesis was carried out in a 500 ml glass reactor equipped with a jacket, reflux condenser, nitrogen gas inlet, thermometer, feeding inlet and a stainless steel anchor stirrer. Nanoclay was first dispersed in DI water in the reactor at 75 °C, after then surfactant and sodium pyrophosphate decahydrate were added under a nitrogen stream. Next, 10% of prepared pre-emulsion was inserted into the reactor. After the exotherm reaction, the left pre-emulsion and catalyst solution was fed at constant rates into the reactor for 4 h at 75 °C. Catalyst solution was dropped into the reactor at 30 min intervals during polymerization. To complete the polymerization, temperature of the reactor was heated at 80 °C for an additional 2 h. After then, the reactor was cooled down under 40 °C. NaOH was used to control pH of final acrylic emulsion PSAs reinforced with nanoclay.

2.3.2. Semibatch emulsion polymerization PSAs mechanically blended with nanoclay

Acrylic pre-emulsion PSAs (2-EHA 45) was synthesized by semibatch emulsion polymerization as mentioned above at 2.2. After then, the reactor was cooled down under 40 °C, nanoclay was charged to reactor and stirred for 1 h. NaOH was used to control pH of final acrylic emulsion PSAs reinforced with nanoclay.

2.4. Analysis of synthesis acrylic emulsion PSAs

2.4.1. Fourier-transform infrared (FT-IR) spectroscopy

To investigate the synthesized five acrylic pre-emulsion PSAs, the PSAs were analyzed by FT-IR spectroscopy. The IR spectra were recorded using JASCO FT/IR-6100 (Japan) equipped with a Miracle accessory, an attenuated total reflectance (ATR). It had a transmission range from 4000 to 650 cm⁻¹. The resolution of the spectra recorded was 8 cm⁻¹. The difference of the five acrylic emulsion PSAs was analyzed by observing the absorbance.

2.4.2. Gel permeation chromatography (GPC)

The weight average molecular weight (M_w), number average molecular weight (M_n) and molecular weight distribution (M_w/M_n , MWD) of the synthesized pre-emulsion PSAs were determined by GPC (Waters, USA). The samples were dissolved in tetrahydrofuran (THF)

at the ratio of 0.5% w/v solutions. GPC was used to obtain narrow molecular weight fractions and separation was accomplished on a column of a highly porous material that separates the polymer molecules according to size.

2.4.3. Modulate differential scanning calorimetry (MDSC)

The T_g of the acrylic pre-emulsion PSAs was measured using MDSC (DSC Q-1000, TA Instrument, USA). MDSC offers all the benefits of standard DSC, overcomes its limitations, and provides further information for greater understanding of material properties. MDSC permits separation of the total heat flow signals into its thermodynamic (heat capacity) and kinetic components. In general, MDSC are used in difficult or impossible measurement by standard DSC. The samples are cooled from room temperature to $-80\text{ }^\circ\text{C}$ and then heated to $50\text{ }^\circ\text{C}$ at a heating rate of $2\text{ }^\circ\text{C}/\text{min}$ in the first scan to remove thermal history. They are cooled again to $-80\text{ }^\circ\text{C}$ and kept the temperature for 1 min, after then heated to $50\text{ }^\circ\text{C}$ at a heating rate of $2\text{ }^\circ\text{C}/\text{min}$ in the second scan. The T_g was taken as the midpoint of the inflection in the second scanned MDSC curve.

2.4.4. X-ray diffraction (XRD)

The XRD analysis of acrylic emulsion PSAs with nanoclay was obtained in an XpertPro diffractometer (Panalytical B.V.Co., Germany) with Ni filtered Cu $K\alpha$ radiation ($\lambda=0.15406\text{ nm}$) at room temperature. The range of the diffraction angle (2θ) is from 2° to 12° with a scanning rate of $0.4\text{ }^\circ/\text{min}$. The spacing of the nanoclay (d) was calculated using the Bragg equation; $n\lambda=2d\sin\theta$, where λ is the wavelength of the X-ray and θ is the scattering half angle.

2.4.5. Field-emission scanning electron microscope (FE-SEM)

The morphological analysis of the nanoclay in the acrylic emulsion PSAs was examined by FE-SEM (JSM 5410LV, JEOL, Japan). The samples were frozen in liquid nitrogen and the freeze-dried. The samples were coated with Au before FE-SEM observation.

2.4.6. Advanced rheometric expansion system (ARES)

The viscoelastic properties of the acrylic emulsion PSAs were determined using ARES (Rheometric Scientific, UK) using 8 mm parallel plate under a liquid nitrogen atmosphere. The measurements were carried out with $3\text{ }^\circ\text{C}/\text{min}$ of heating rate and 1 Hz of frequency. Dried PSA films with 2 mm thickness were subjected to a temperature sweep from $-80\text{ }^\circ\text{C}$ to $160\text{ }^\circ\text{C}$.

2.4.7. Adhesion performances

Acrylic PSAs were coated onto a corona treated 25- μm -thick polyethylene terephthalate film (PET, SKC Co. Ltd., Republic of Korea) using no. 26 bar and coated films were dried in a convection oven at $110\text{ }^\circ\text{C}$ for 5 min. The dried PSA layers on the PET film were about 50 μm thickness. The PSA tapes were stored at $25\text{ }^\circ\text{C}$ and 50% relative humidity (RH) for 24 h before the adhesion performance test.

2.4.7.1. 180° Peel strength. The peel strength was also measured using a universal testing machine (UTM, Zwick, Z101, Germany). The specimen for peel strength test was cut into 25 mm width, attached to stainless steel substrate and then 2 kg rubber roller was passed two times to press onto the stainless steel substrate. After keeping the specimen at room temperature for 24 h, the measurements were carried out at an angle of 180° between the substrate and PSA specimen with a crosshead speed of 300 mm/min at room temperature. The force was recorded in g during five different runs, and the average value was recorded in g .

2.4.7.2. Probe tack. Tack measurements of PSA films were carried out with a TA-XT2i Texture Analyzer (Micro Stable Systems, UK) at $20\text{ }^\circ\text{C}$ using a probe tack which was a polished stainless steel cylinder probe with 5 mm diameter. Probe approached with the 0.5 mm/s of crosshead speed and then contacted with the surface of PSA films with a constant pressure of $100\text{ g}/\text{cm}^2$ for 1 s and then separated from the surface with the speed of 0.5 mm/s.

2.4.7.3. Shear adhesion failure temperature (SAFT). For the SAFT, the PSA samples were pressed onto stainless steel (bonding area $25 \times 25\text{ mm}^2$) by two passes of a 2 kg rubber-roller. The specimen was placed in an oven, and then a 500 g and 1 kg weight was hung from the end of the sample. The temperature-dependent pull away of the PSA sample from the plate was detected in heating oven at temperatures ranging from room temperature to $200\text{ }^\circ\text{C}$ at a heating rate of $0.4\text{ }^\circ\text{C}/\text{min}$.

3. Results and discussions

3.1. Depending on 2-EHA weight percentages

To study the influence of the 2-EHA/BA ratio on the adhesive performance, a series of acrylic emulsion PSAs were synthesized with a batch polymerization process at a different 2-EHA/BA ratio based on the weight of the total monomer.

3.1.1. FTIR spectroscopy

To investigate the synthesized acrylic emulsion PSAs, the FTIR-ATR spectra of five series of acrylic emulsion PSAs are shown in Figs. 1–3. The broad peak at 3380 cm^{-1} is related to the absorbing peak of hydroxyl group (OH). The absorbance band at 2957 and 2874 cm^{-1} can be assigned to the CH_3 stretch vibration of alkyl group (Fig. 2). 1730 cm^{-1} is the $\text{C}=\text{O}$ stretch vibration of acrylate. Peaks at 1448 and 1387 cm^{-1} are the CH_2 - bending mode. Peaks at 1254, 1171 and 1121 cm^{-1} are $\text{C}-\text{O}-\text{C}$ stretch vibrating absorbing peaks [22,23]. FT-IR illustrated that polymerization of all the acrylic emulsion PSAs had done successfully. The heights of absorbance by acrylate group and alkyl group are different because of different molecular weight of 2-EHA and BA. As the weight percentage of 2-EHA increased, the alkyl groups peak increased. For the same reason, decreasing 2-EHA weight percentage of total monomer had acrylate peak at 1730, 1254, 1171 and 1121 cm^{-1} increased (Fig. 3).

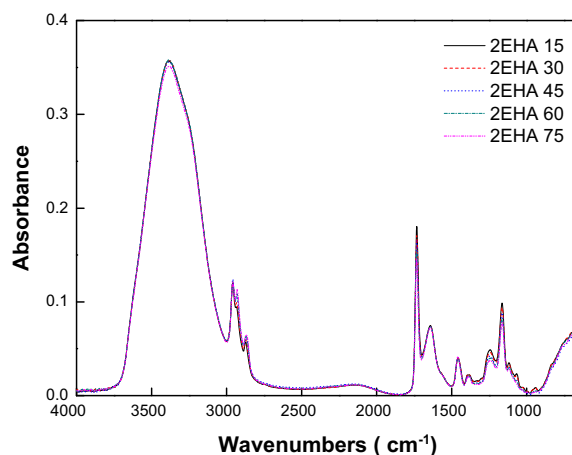


Fig. 1. FT-IR spectrum of pre-emulsion PSAs as a function of 2-EHA/BA ratio.

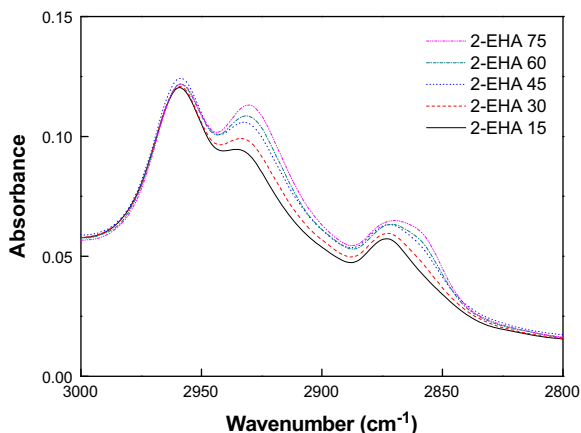


Fig. 2. Changes in the absorbance peaks of the alkyl group (2957 and 2874 cm^{-1}) as a function of 2-EHA/BA ratio.

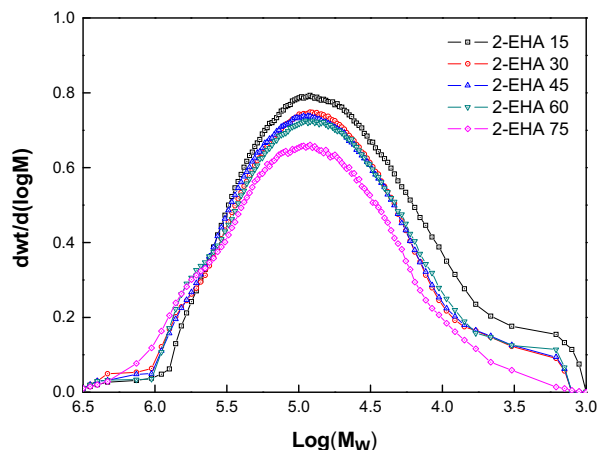


Fig. 4. Molecular weight distributions for pre-emulsion PSAs as a function of 2-EHA/BA ratio.

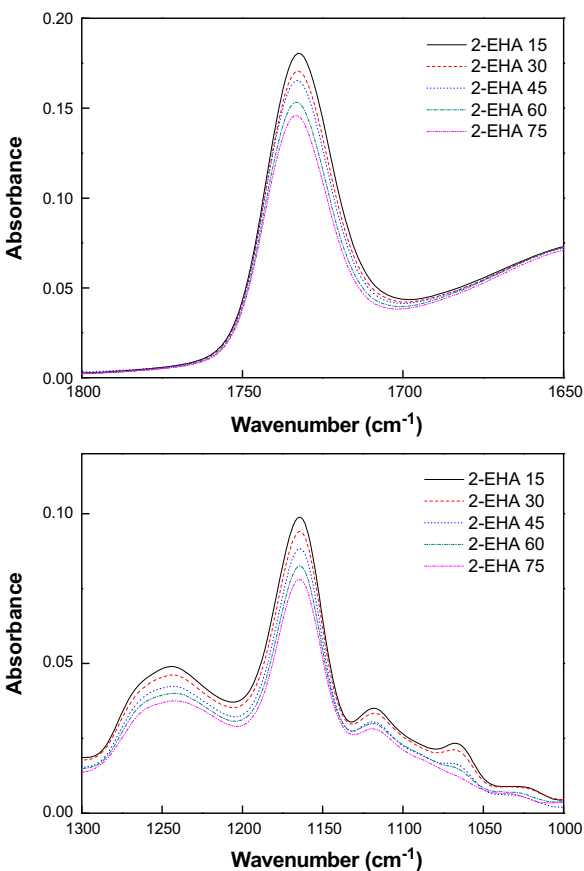


Fig. 3. Changes in the absorbance peaks of the alkylate group (1730, 1254, 1171 and 1121 cm^{-1}) as a function of 2-EHA/BA ratio.

3.1.2. GPC

M_w of acrylic emulsion PSAs are presented in Fig. 4. M_n and M_w are listed in Table 3. GPC data indicates that M_w of the acrylic emulsion PSAs increased with increasing 2-EHA concentration because of chain transfer. 2-EHA brings out higher chain transfer to monomer by the propagation. Decrease of M_w made polymer mobility higher in the acrylic emulsion PSAs and peel strength increased for that reason. On the other hands, acrylic emulsion PSAs which had too lower molecular weight shows lower peel strength because of entanglement reduction as shown in Fig. 6.

Table 3
The characterization of acrylic emulsion PSAs.

	2-EHA 15	2-EHA 30	2-EHA 45	2-EHA 60	2-EHA 75
M_n^a	36 K	32 K	32 K	38 K	33 K
M_w^a	130 K	140 K	140 K	170 K	220 K
MWD ^a	3.4	4.5	4.4	4.6	6.7

^a Measured by GPC.

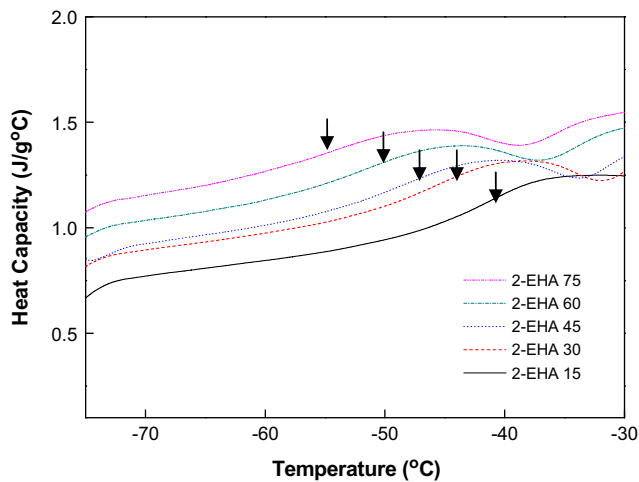


Fig. 5. MDSC thermogram and T_g of the pre-emulsion PSAs.

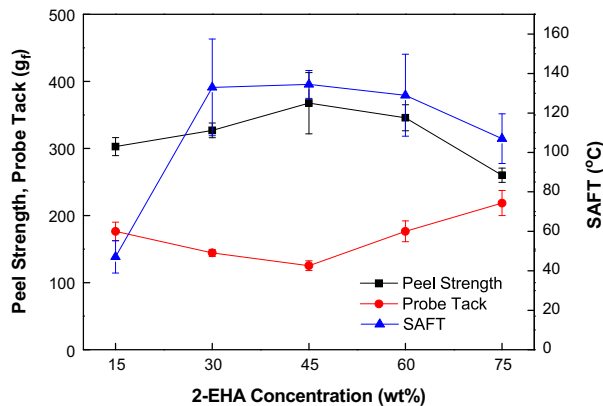


Fig. 6. Peel strength, probe tack and SAFT of the pre-emulsion PSAs as a function of 2-EHA concentrations.

3.1.3. MDSC

The characteristics of acrylic emulsion PSAs can be determined by controlling the monomer composition. The solid contents and T_g of the five 2-EHA series PSAs are shown in Table 4. The solid contents of prepared acrylic emulsion PSAs were determined by weight calculation of before and after drying of samples.

Fig. 5 presents T_g curves by MDSC for five acrylic emulsion PSAs. The nano-composites do not show clear glass transition temperature because of the intercalated polymer chains within the silicate spacing that prevent the segmental motions of the polymer chains [24]. As increasing the 2-EHA content, the T_g of PSAs gradually decreased because T_g of the 2-EHA is lower than BA.

3.1.4. Adhesion performance of acrylic pre-emulsion PSAs

In the acrylic emulsion PSAs, monomer composition greatly influences their adhesion performances such as peel strength, tack and SAFT.

The peel strength of the acrylic emulsion PSAs showed maximum peak with increase of 2-EHA contents. After that, peel strength was decreased with increasing 2-EHA contents. Probe tack values present an opposite results compared with that of peel strength as shown in Fig. 6. The acrylic emulsion PSAs which 2-EHA/BA ratio was 45/45 showed the highest value of peel strength and 2-EHA/BA ratio was 75/15 showed the lowest value of that. A maximum value of the shear strength is revealed at 30/60 of 2-EHA/BA ratio. The introduction of a greater number of 2-EHA structural units to the polymer chains made the polymer soft, with an increment of tack and a loss of peel strength. However, the inter-reaction of rigid polymer chains at the interface of particle-particle is more difficult, because of the decrease of the mobility of polymers. At the point which 2-EHA contents was over 45 wt%, the interfacial adhesion between the particles decreased and the film shows decreasing adhesion performances, which promotes the development of fractures and the material decohesion. This decohesion produces also a complete loss of shear strength.

Table 4
Solid contents and T_g of acrylic pre-emulsion PSAs.

	2-EHA 15	2-EHA 30	2-EHA 45	2-EHA 60	2-EHA 75
Solid contents (wt%)	54.3	53.8	54.6	54.2	54.5
T_g (°C) ^a	-41.1	-45.5	-48.2	-51.9	-55.5

^a Measured by MDSC.

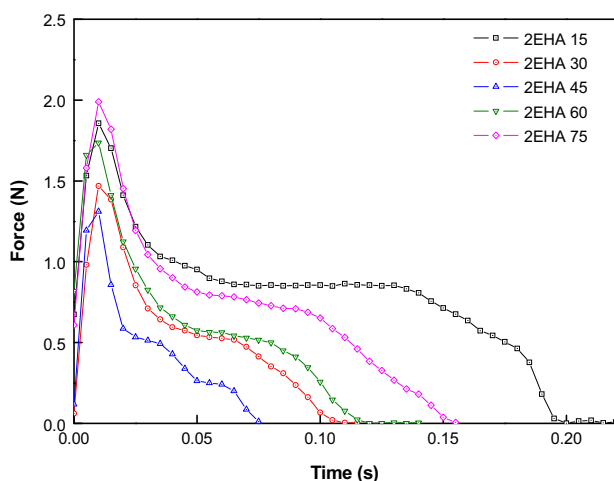


Fig. 7. Stress-strain curve of the pre-emulsion PSAs as a function of 2-EHA concentration.

Fig. 7 shows a typical stress-strain curve during the debonding process of probe tack test. The strain is obtained by dividing the crosshead displacement by the thickness of the film and the stress is obtained by dividing the force by the actual contact area. For example, the curve presents a sharp stress maximum and adhesive debonding at comparatively low strains. It has a similar shape as the stress strain plots of brittle polymeric materials in the usual tensile tests. In this study, a similar behavior was observed for 2-EHA 45. On the other hands, if the stress maximum was caused by the fibrils debonded from the probe surface by interfacial fracture, a large area under the curve and a high strain at break are observed, the PSAs have similarity with plastic deformation.

3.2. Depending on preparation method of emulsion PSAs reinforced with nanoclay

The all results of five acrylic pre-emulsion PSAs revealed that 45/45 of 2-EHA/BA ratio have good balance between adhesion and cohesion.

It is well known that lots of properties of polymer can be improved by adding much lower amount of clay. There are different processes to make PSA/clay nano-composites. In order to study the influence of the loading nanoclay on the adhesion properties, PSA/clay nano-composites were prepared by *in-situ* polymerization and mechanical blending.

3.2.1. Morphological observation

The morphology of polymer-clay nano-composites was analyzed by XRD and SEM. The degree of intercalation and dispersion of the clay in the PSA matrix were obtained by the two methods. XRD patterns of clay, pure PSA, PSA-clay nano-composites by *in-situ* polymerization and mechanical blending were measured. All the results are shown in Fig. 8. From XRD pattern, the d -spacing were calculated from Bragg formula, at peak positions. Because of crystal structure of nanoclay, the diffraction peak of Na-MMT is appeared at $2\theta = 7.3^\circ$ [25]. The interlayer space of $d = 12.1$ nm is calculated from diffraction peak position.

XRD patterns for PSA-clay nano-composites by *in-situ* polymerization had similar tendency compared to pure PSA. It means no crystallinity, that is, nanoclay is well-dispersed in PSA matrix. The other side, XRD patterns of the PSA-clay nano-composites by mechanical blending showed diffraction peak in the range of 3.47° , which corresponds to an interlayer space of $d = 25.4$ nm, indicating

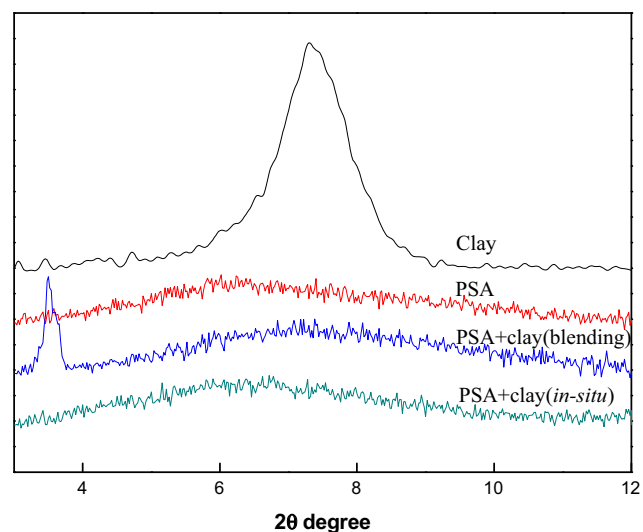


Fig. 8. XRD patterns of Na-MMT, PSA and PSA-clay nano-composites by mechanical blending and *in-situ* polymerization.

that Na-MMT in the PSA matrix was intercalated, not exfoliated [25]. Due to the intercalation of nanoclay, the space between layered silicates of PSA–clay nano-composites increased from 12.1 nm to 25.4 nm.

The difference between dispersion microstructure and dispersed phase of PSA–clay nano-composite by *in-situ* polymerization and mechanical blending was also examined by SEM micrographs. The XRD and SEM measurements are regarded as complementary method to each other for the characterization of the PSA–clay nano-composites [26]. Fig. 9 shows the SEM micrographs of PSA–clay nano-composites by mechanical blending and *in-situ* polymerization, where the white lines present the Na-MMT and dark part is the PSA matrix. In Fig. 9(a), the silicate layers of nano-composites by mechanical blending are intercalated, positioned in good order. Exfoliated state of nanoclay dispersed in PSA–clay nano-composites by *in-situ* polymerization can be observed in Fig. 9(b). The layered silicates morphology of PSA–clay nano-composites was different according to preparation method, which is associated with XRD analysis by the SEM micrographs.

3.2.2. Viscoelastic properties

Glass transition temperature, T_g , was analyzed by MDSC and shown in Fig. 10. A negligible increase in T_g was observed for the PSA–clay nano-composites by *in-situ* polymerization and mechanical blending compared to pure PSA (Fig. 10). The origin of effect on T_g is not clear and remains a subject of future study [27]. The T_g is important for PSA in application field because an increment in the

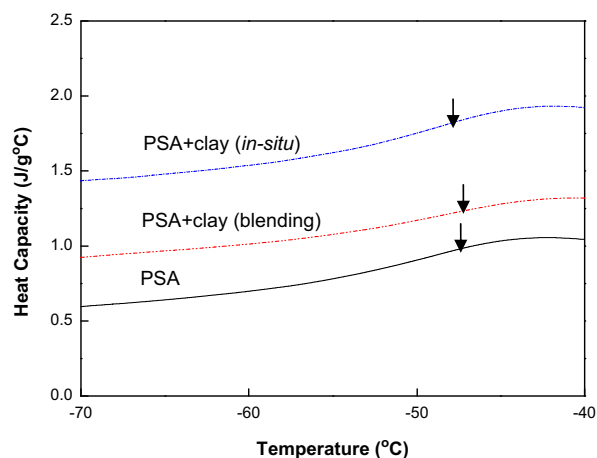


Fig. 10. MDSC thermogram and T_g of the pure PSA and PSA–clay nano-composites.

T_g might affect the film formation temperature in a deleterious way [25].

The viscoelastic behaviors of the pure PSA, PSA–clay nano-composites by *in-situ* polymerization and mechanical blending with 1 wt% of Na-MMT clay were evaluated and compared with each other using ARES analysis. The viscoelastic behavior of pure PSA and PSA–clay nano-composites are related to their properties. The storage modulus (G') means the elastic deformation of PSA material and adhesive hardness at a specific temperature and frequency. In Fig. 11, storage modulus (G') in temperature range -70 to 160 °C at frequency 1 Hz for pure PSA and two kinds of nano-composites are presented. The curves as a function of temperature are typical for amorphous polymers. The storage modulus of the two kinds of nano-composites were higher than that of the pure PSA above 0 °C. Moreover, storage modulus of the *in-situ* polymerized PSA–clay nano-composites is higher than that of the PSA–clay nano-composites by mechanical blending. Above T_g , when the PSA becomes soft, the reinforcement effect of the clay is significant owing to the restricted movement of polymer chains surrounding the clay. In other words, the storage modulus was improved in the rubbery plateau by layered silicate. These observations can be related to the strong interfacial interactions between the PSA matrix and layered silicates, Na-MMT, which are normally observed in rubber composites [28,29]. The increase in storage modulus is associated with increased adhesion performance of PSA–clay nano-composites.

3.2.3. Adhesion performance

Adhesion performance of pure PSA, two kinds of nano-composites was shown in Figs. 12–14. The *in-situ* polymerized PSA–clay nano-composites exhibit higher adhesion performance, especially SAFT, compared to the pure PSA. The increment of the adhesion performance can be explained by the rigidity of the PSA–clay nano-composites caused by the presence of inserted polymer chains in the interlayer of clay. On the other hands, PSA–clay nano-composites by mechanical blending show low adhesion performances. This is associated with XRD and FE-SEM analysis, where exfoliated the Na-MMT was not observed for nano-composites by a mechanical blending. Beall and Tspirisky concluded that the unexfoliated platelets can act as stress concentrators, contributing to a decreased some properties of nano-composites [30].

4. Conclusions

A series of water-borne adhesives based on 2-ethylhexyl acrylate (2-EHA), *n*-butyl acrylate (BA), methylmethacrylate (MMA)

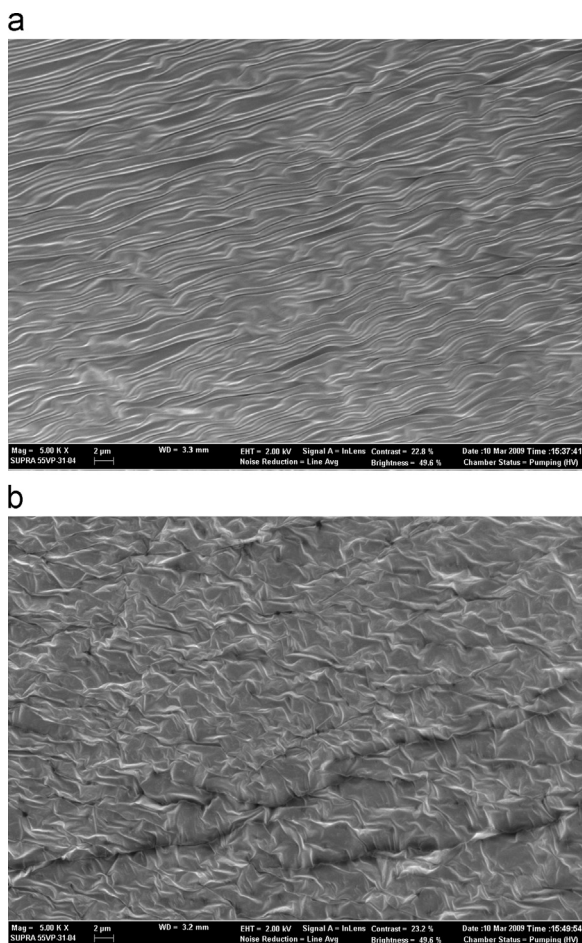


Fig. 9. FE-SEM micrographs of PSA–clay nano-composites by (a) mechanical blending and (b) *in-situ* polymerization.

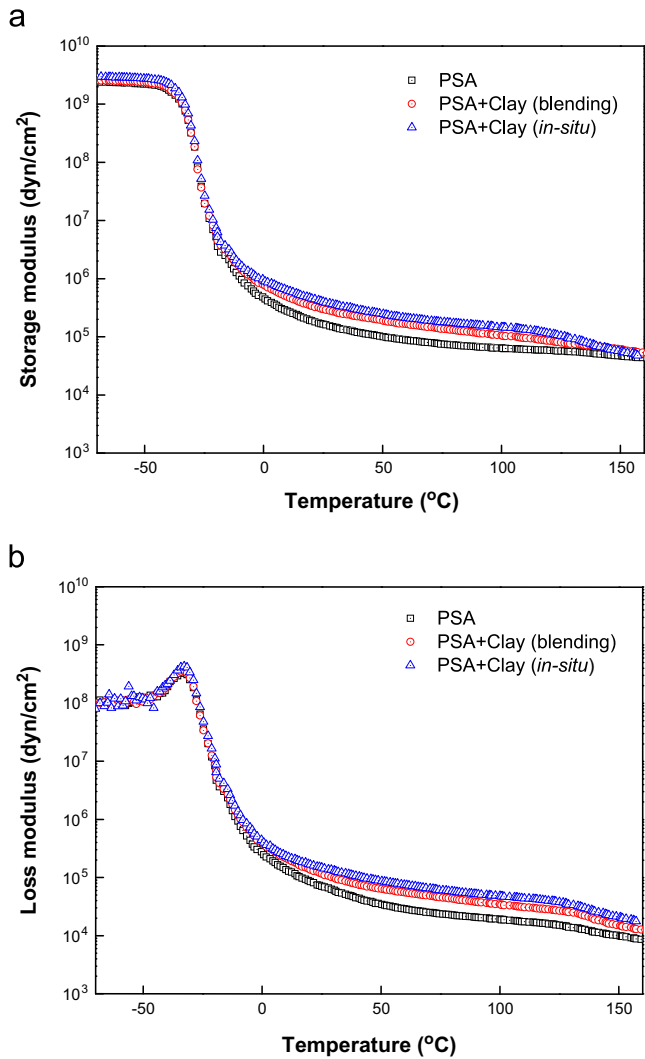


Fig. 11. Temperature dependence of storage modulus (a) and loss modulus (b) for PSA and two kinds of nano-composites.

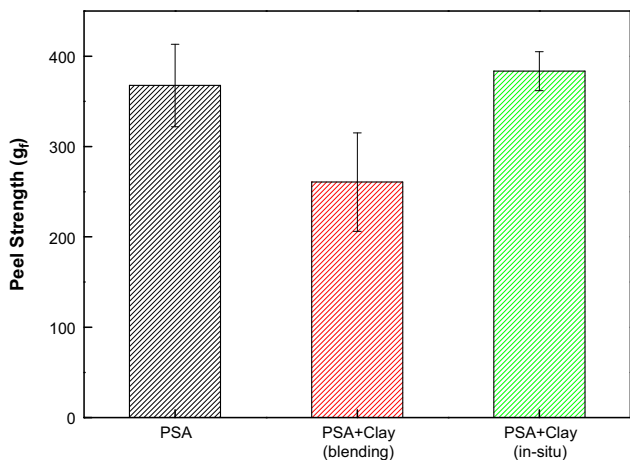


Fig. 12. Peel strength of PSA, PSA–clay nano-composites by *in-situ* polymerization and mechanical blending.

and acrylic acid (AA) copolymers were synthesized by semicontinuous emulsion polymerization. Different 2-EHA/BA ratios have an influence on adhesion performances. The T_g of the acrylic emulsion PSAs decreased because of Higher amounts of 2-EHA thereby

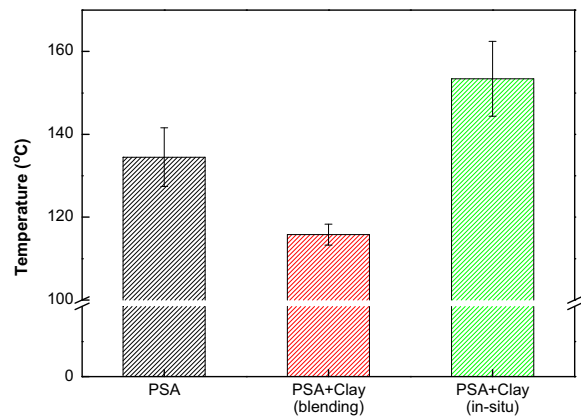


Fig. 13. Shear adhesion failure temperature (SAFT) of PSA, PSA–clay nano-composites by *in-situ* polymerization and mechanical blending.

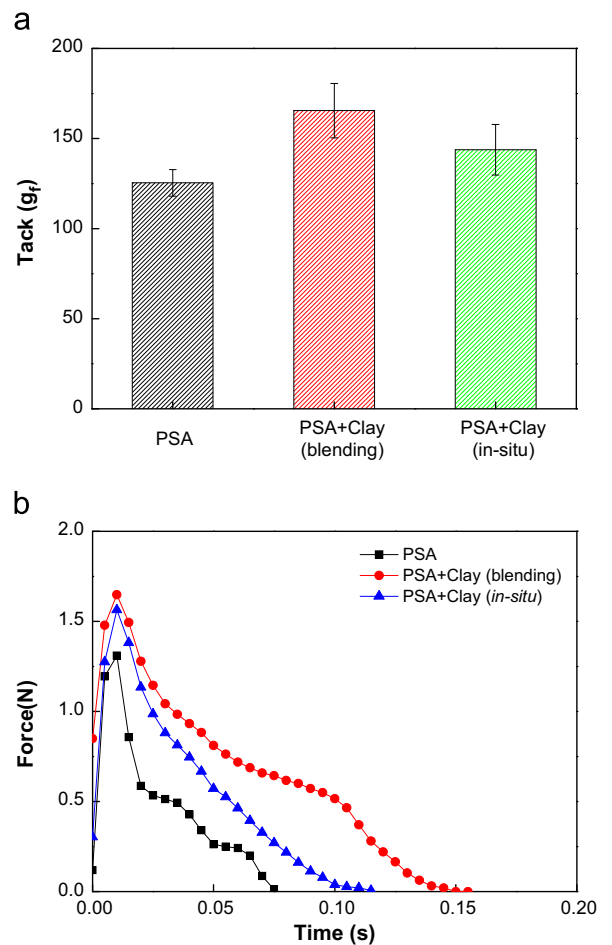


Fig. 14. (a) Probe tack and (b) stress–strain curve of PSA, PSA–clay nano-composites by *in-situ* polymerization and mechanical blending.

adhesion performances were changed. The measurements of the peel strength, probe tack and SAFT as a function of the 2-EHA/BA ratio revealed good adhesion performances when 2-EHA/BA ratio was 45/45 wt%.

Acrylic emulsion PSAs/clay nano-composites were synthesized by *in-situ* emulsion polymerization and mechanical blending with pristine Na-MMT as layered silicate. XRD and FE-SEM demonstrated that the dispersion of the nanoclay by mechanical blending in PSA matrix is worse than that of *in-situ* polymerization. Only PSA–clay nano-composites by *in-situ* polymerization have

exfoliated structures. Viscoelastic properties characterization of pure PSA and PSA–clay nano-composites using ARES analysis showed an increase in storage modulus, which is related with adhesion performance with loading nanoclay. The results have been shown that PSA–clay nano-composites by mechanical blending was compared well with *in-situ* emulsion polymerization through measuring adhesion performances, peel strength, probe tack and SAFT.

References

- [1] Tobing SD, Klein A. Molecular parameters and their relation to the adhesive performance of emulsion acrylic pressure-sensitive adhesives. II. Effect of crosslinking. *Journal of Applied Polymer Science* 2001;79(14):2558–64.
- [2] Gower M, Shanks R. The effect of varied monomer composition on adhesive performance and peeling master curves for acrylic pressure-sensitive adhesives. *Journal of Applied Polymer Science* 2004;93(6):2909–17.
- [3] Moayed SH, Fatemi S, Pourmahdian S. Synthesis of a latex with bimodal particle size distribution for coating applications using acrylic monomers. *Progress in Organic Coatings* 2007;60(4):312–9.
- [4] Tan HS, Pfister WR. Pressure-sensitive adhesives for transdermal drug delivery systems. *Pharmaceutical Science & Technology Today* 1999;2(2):60–9.
- [5] Wang T, Lei CH, Dalton AB, Creton C, Lin Y, Fernando KAS, et al. Waterborne, nanocomposite pressure-sensitive adhesives with high tack energy, optical transparency, and electrical conductivity. *Advanced Materials* 2006;18(20):2730–4.
- [6] Li H, Yang Y, Yu Y. Acrylic emulsion pressure-sensitive adhesives (PSAS) reinforced with layered silicate. *Journal of Adhesion Science and Technology* 2004;18(15–16):1759–70.
- [7] Zerda AS, Lesser AJ. Intercalated clay nanocomposites: morphology, mechanics, and fracture behavior. *Journal of Polymer Science Part B: Polymer Physics* 2001;39(11):1137–46.
- [8] Luo JJ, Daniel IM. Characterization and modeling of mechanical behavior of polymer/clay nanocomposites. *Composites Science and Technology* 2003;63(11):1607–16.
- [9] Chin I-J, Thurn-Albrecht T, Kim H-C, Russell TP, Wang J. On exfoliation of montmorillonite in epoxy. *Polymer* 2001;42(13):5947–52.
- [10] Greesh N, Hartmann PC, Cloete V, Sanderson RD. Impact of the clay organic modifier on the morphology of polymer–clay nanocomposites prepared by *in situ* free-radical polymerization in emulsion. *Journal of Polymer Science Part A: Polymer Chemistry* 2008;46(11):3619–28.
- [11] Lan T, Pinnavaia TJ. Clay-reinforced epoxy nanocomposites. *Chemistry of Materials* 1994;6(12):2216–9.
- [12] Meneghetti P, Qutubuddin S. Synthesis, thermal properties and applications of polymer–clay nanocomposites. *Thermochimica Acta* 2006;442(1–2):74–7.
- [13] LeBaron PC, Wang Z, Pinnavaia TJ. Polymer-layered silicate nanocomposites: an overview. *Applied Clay Science* 1999;15(1):11–29.
- [14] Ellis TS, D'Angelo JS. Thermal and mechanical properties of a polypropylene nanocomposite. *Journal of Applied Polymer Science* 2003;90(6):1639–47.
- [15] Shen Z, Simon GP, Cheng Y-B. Comparison of solution intercalation and melt intercalation of polymer–clay nanocomposites. *Polymer* 2002;43(15):4251–60.
- [16] Alexandre M, Dubois P. Polymer-layered silicate nanocomposites: preparation, properties and uses of a new class of materials. *Materials Science and Engineering R: Reports* 2000;28(1):1–63.
- [17] Sinha Ray S, Okamoto M. Polymer/layered silicate nanocomposites: a review from preparation to processing. *Progress in Polymer Science* 2003;28(11):1539–641.
- [18] Meneghetti P, Qutubuddin S, Webber A. Synthesis of polymer gel electrolyte with high molecular weight poly (methyl methacrylate)–clay nanocomposite. *Electrochimica Acta* 2004;49(27):4923–31.
- [19] Wang D, Zhu J, Yao Q, Wilkie CA. A comparison of various methods for the preparation of polystyrene and poly (methyl methacrylate) clay nanocomposites. *Chemistry of Materials* 2002;14(9):3837–43.
- [20] Xu Y, Brittain WJ, Xue C, Eby RK. Effect of clay type on morphology and thermal stability of PMMA–clay nanocomposites prepared by heterocoagulation method. *Polymer* 2004;45(11):3735–46.
- [21] Tiwari RR, Natarajan U. Thermal and mechanical properties of melt processed intercalated poly (methyl methacrylate)–organoclay nanocomposites over a wide range of filler loading. *Polymer International* 2007;57(5):738–43.
- [22] Lu SH, Liang GZ, Wang JL, Ren HJ. Synthesis and performance characteristics of a water-based polyacrylate microemulsion for UHMWPE fiber adhesive coating. *Journal of Applied Polymer Science* 2006;99(6):3195–202.
- [23] Seo Y-O, Seul S-D. Studies on the synthesis and characteristic of removal type pressure-sensitive acrylic adhesives. *Journal of Korean Industrial and Engineering Chemistry* 2000;11(3):335–40.
- [24] Lee DC, Jang LW. Preparation and characterization of PMMA–clay hybrid composite by emulsion polymerization. *Journal of Applied Polymer Science* 1998;61(7):1117–22.
- [25] Diaconu G, Paulis M, Leiza JR. Towards the synthesis of high solids content waterborne poly(methyl methacrylate-co-butyl acrylate)/montmorillonite nanocomposites. *Polymer* 2008;49(10):2444–54.
- [26] Tjong S. Structural and mechanical properties of polymer nanocomposites. *Materials Science and Engineering R: Reports* 2006;53(3):73–197.
- [27] Huang X, Brittain WJ. Synthesis and characterization of PMMA nanocomposites by suspension and emulsion polymerization. *Macromolecules* 2001;34(10):3255–60.
- [28] Maiti S, De S, Bhowmick AK. Quantitative estimation of filler distribution in immiscible rubber blends by mechanical damping studies. *Rubber Chemistry and Technology* 1992;65(2):293–302.
- [29] Satas D. Handbook of pressure sensitive adhesive technology. Van Nostrand Reinhold; 1989.
- [30] Al-Malaika S, Golovoy A, Wilkie CA. Chemistry and technology of polymer additives. Blackwell Science; 1999.